ADVANCED MATERIALS INTERFACES
www.advmatinterfaces.de

# Plasma-Assisted Deposition of $TiO_2$ 3D Nanomembranes: Selective Wetting, Superomniphobicity, and Self-Cleaning

*Laura Montes, Jose M. Román, Xabier García-Casas, Javier Castillo-Seoane, Juan R. Sánchez-Valencia, Ángel Barranco, Carmen López-Santos,* and Ana Borrás**

**Fabrication of tunable wetting surfaces is sought for the last years given its importance on energy, biomaterials and antimicrobials, water purification, microfluidics, and smart surfaces. Liquid management on surfaces mainly depends on the control at the micro- and nanoscale of both roughness and chemical composition. Herein, the combination of a soft-template method and plasma-enhanced chemical vapor deposition is presented for the synthesis of $TiO_2$ nanofibers on porous substrates such as cellulose and stainless-steel membranes. The protocol, carried out under mild conditions, produces 3D nanomembranes with superhydrophobicity and oleophilicity that are tested as microliter water/oil filters. Photoactivation of $TiO_2$ by UV illumination provides a straightforward approach for wetting tunability that converts the surface into amphiphilic. A final chemical modification of the $TiO_2$ nanofibers by embedding them in an elastomeric polymeric shell and by fluorine-based grafting opens the path toward the formation of superomniphobic and self-cleaning surfaces with long-lasting lifetimes. Thus, a reliable procedure is demonstrated for the fabrication of $TiO_2$ nanofibers, which allows the modification of porous supports and provides an innovative route for the development of 3D nanomembranes with under design wetting. This protocol is extendable to alternative metal oxides, metals, and core@shell nanoarchitectures with potential multifunctionalities.**

## 1. Introduction

In 2015, the United Nations' Members adopted the agenda for sustainable development, including 17 global goals to achieve before 2030. Sustainable Development Goal number 6 (SDG6) is entitled Clean Water and Desalination. Indeed, the increasingly frequent periods of water shortage[1] together with pollution from industrial and pesticide spills[2] and the presence of emergent pollutants[3] are a great deal responsible for the scarcity of clean water that affects about 40% of the world population. Such a situation calls for the development of new methods of obtaining safe drinking water, which must be answered from scientific, commercial, and social concerns.[4] From the scientific point of view, water treatment and separation techniques such as flotation, gravity separation, reverse osmosis, and photocatalytic removal of contaminants[5] have been optimized in the last decades. Yet, these are often ineffective against emergent pollutants such as microplastics or when dealing with small amounts of liquid. However, the latter case is crucial in research fields also related to the SDGs, such as energy, as well as in microfluidics, microbiology, food packaging,[6] or pharmacy to isolate and separate substances and/or microorganisms from effluents.[7] In this context, the advance of systems for small volume liquid separation is an important issue in nanotechnology and science materials research. Liquid separation is usually carried out utilizing a membrane[4,8] of very small thickness compared to its surface which, when interposed between two fluid phases, makes a selective control of the mater and/or energy transfer between them.[9] In some cases, it acts as a repellent or shield from pollutants in suspension whereas in other cases, the membrane can be an extracting agent for harmful substances or promoting the transport of degradation compounds.[10] To evaluate the functionality of a membrane, the material, pore size, geometry, and distribution, as well as other physical–chemical properties such as density and surface tension, must be taken into account.[11] For microfluidics, nanodevices are employed thanks to a high response rate working in both passive and active modes of separation techniques.[12] Particularly, hydrophilic membranes (affinity to be wet by water)[13] are used for gravity filtration of emulsions due to their clogging resistance. However, they are not suitable for separating water-in-oil emulsions since liquids can easily permeate through them. Therefore, an ideal membrane model would be hydrophilic and oleophobic (repulsion against nonpolar liquids) working in both air and underwater environments. An additional problem is that the oleophobic membranes frequently lose this property

L. Montes, J. M. Román, X. García-Casas, J. Castillo-Seoane, J. R. Sánchez-Valencia, Á. Barranco, C. López-Santos, A. Borrás
Institute of Materials Science of Seville (US-CSIC) Americo Vespucio 49 Seville 41092, Spain
E-mail: mclopez@icmse.csic.es; anaisabel.borras@icmse.csic.es
J. Castillo-Seoane, J. R. Sánchez-Valencia
Atomic, Nuclear and Molecular Physics Department
Facultad de Física
University of Seville
Ad. Reina Mercedes s/n, Seville 41012, Spain
C. López-Santos
Department of Applied Physics I
University of Seville
Virgen de Africa, Seville 41011, Spain
The ORCID identification number(s) for the author(s) of this article can be found under https://doi.org/10.1002/admi.202100767.



**DOI: 10.1002/admi.202100767**

upon immersion in water.[14] On the other hand, when the characteristic dimensions or porous sizes are in the nanoscale, the nanomembranes can be applied as high-efficiency cathodes of lithium batteries,[15] contaminated water filtration processes,[16] or in semiconductor-based electronic devices, nanotubes, or graphene,[17] constituting a new concept of "fast flexible electronic."[18] Finally, nanomembranes can also provide highly selective wetting of interest in applications ranging from self-cleaning windows or antifog glass to bactericidal or antiseptic coatings.[19] Nevertheless, their use implies a low flow of filtering, low permeability of oils accompanied by the need to use surfactants.[20]

Framed in this context, we present herein a promising alternative for the manufacturing of multifunctional 3D nanomembranes by the combination of a soft-template protocol based on the use of single-crystalline organic nanowires (ONWs) as vacuum processable 1D templates and the plasma-enhanced chemical vapor deposition (PECVD) of $TiO_2$ nanofibers (NFs) on high-porosity and roughness supports, such as cellulose and stainless steel (SS) filters. These are commercially available supports widely applied in water management and treatment. We show how the surface functionalization of these porous materials confers controlled wetting behavior, highly selective, and tunable under UV illumination. Besides, we demonstrate a novel strategy for the separation of small volumes of emulsions composed of polar and nonpolar liquids by gravity and surface tension effects. An exhaustive analysis of the selective wetting properties of these porous materials decorated with nanostructures as well as its superhydrophobic-to-superhydrophilic conversion under UV irradiation enables its applied possibilities as filtration systems or microfluidic valves. Finally, the chemical modification of the $TiO_2$ nanomembranes with fluorine and their embedding in elastomeric polydimethylsiloxane (PDMS), but keeping the particular three-scale roughness, will provide the production of manageable, reliable, and long-lasting self-cleaning surfaces.

## 2. Results and Discussion

### 2.1. Characterization of the $H_2Pc@TiO_2$ 3D Nanomembranes

Experimental details and the multistep fabrication procedures for the synthesis of the 3D nanomembranes are gathered in the "Experimental Section" and **Scheme 1**. Henceforth, we will use the label $H_2Pc@TiO_2$ NFs to address the formation of core@shell

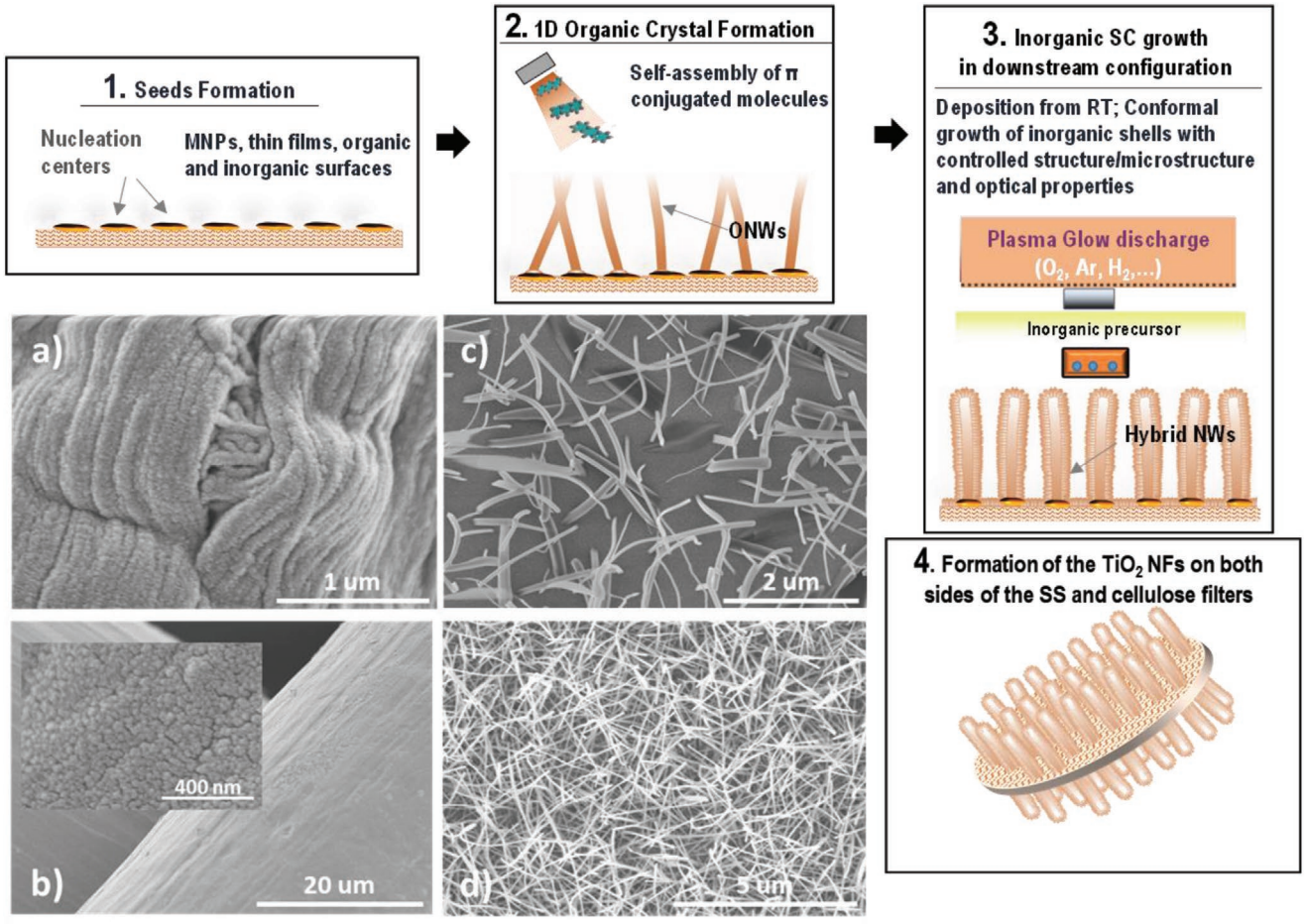


**Scheme 1.** Plasma-assisted deposition of core@shell NFs on 3D supports. Steps 1–4: Pictorial representation of the multistep procedure for the formation of the $H_2Pc@TiO_2$ nanofibers on flat and 3D supports. a,b) Characteristic SEM images of a) the cellulose filter and b) stainless steel membrane after the conformal PECVD of the $TiO_2$ acting as a nucleation layer for the formation of the NFs (step 1). c,d) Top view SEM images of the $H_2Pc$ single-crystalline nanowires growing from the $TiO_2$ nucleation layer for two different densities (step 2).

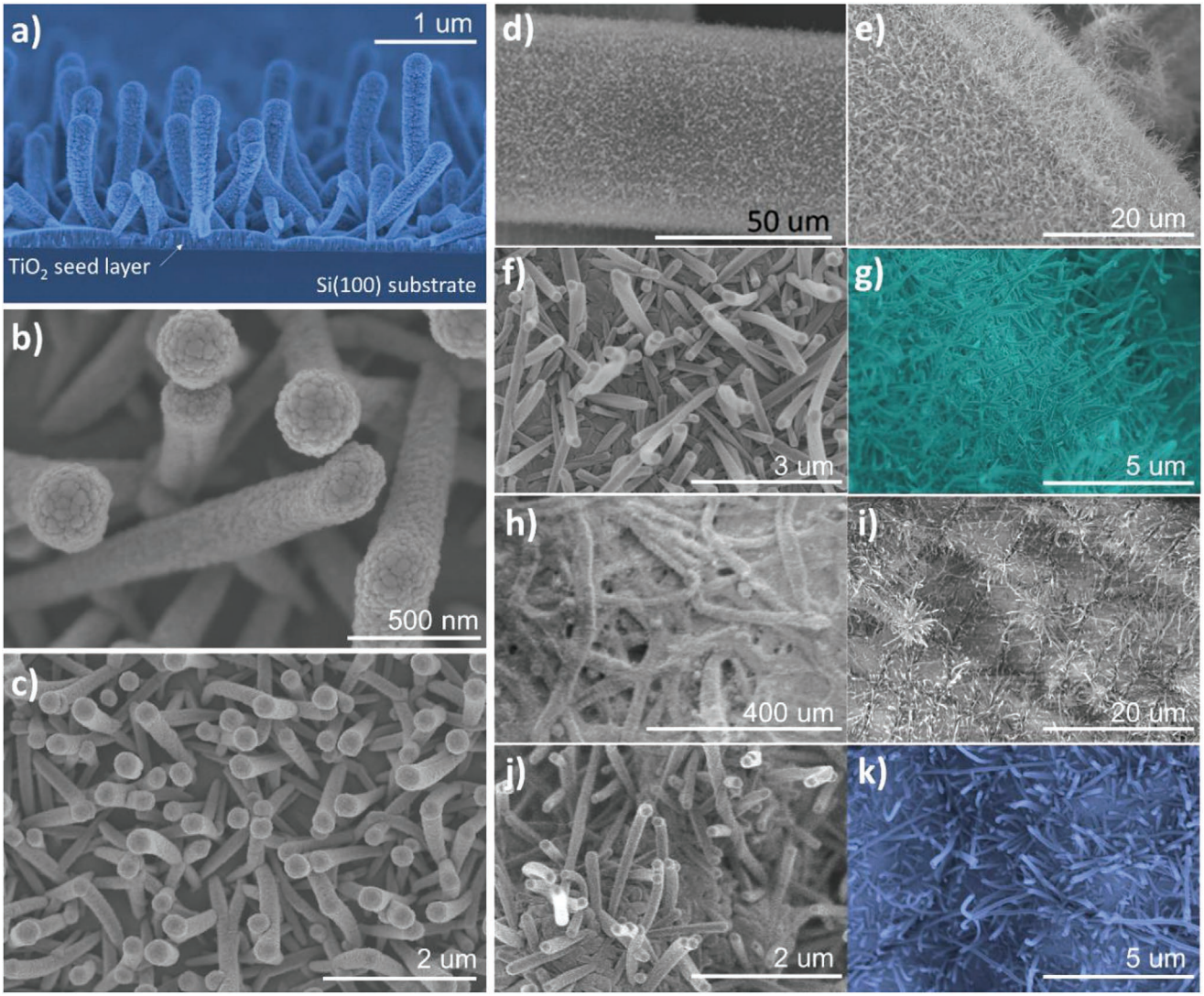


**Figure 1.** Formation of $H_2Pc@TiO_2$ NFs on reference and 3D substrates. Characteristic SEM images at different magnifications of the a–c) $H_2Pc@TiO_2$ NFs deposited onto Si (100), d–g) a stainless steel grid, and h–k) on the 25 µm cellulose membrane. Please note that all the substrates were previously coated with a thin layer of $TiO_2$ as shown in Scheme 1.

NFs using $H_2$-phthalocyanine ($H_2Pc$) as the core and $TiO_2$ as the shell. **Figure 1** gathers characteristic scanning electron microscopy (SEM) images of the growth of $H_2Pc@TiO_2$ NFs on a–c) flat and d–k) 3D supports showing that the proposed synthetic approach is compatible with the formation of a high density of NFs decorating both the cellulose and SS membranes. There are slight differences regarding the density, thickness, and length of the nanofibers for the different supports that can be related to small variations in surface temperature and the higher surface area corresponding to the membranes. For both, the metallic grid and cellulose filters, the NFs present length and diameter distributions depicting a positive skewness curve with the maxima near 4 µm/0.20 and ranging from 2 to 9 µm/0.10–0.35 µm for the length/diameters, respectively (see the "Experimental Section" for further details). Despite such diversity, the SEM images show that the NFs grow with a fine homogeneity in density on the three types of substrates, and the $TiO_2$ shell keeps its characteristic globular and cauliflower-like microstructures. On the other hand, the vertical alignment of the nanofibers after the formation of the $TiO_2$ shell[21] is more pronounced for the Si(100) substrate (Figure 1a), although the side views of the stainless steel grid in panels (e) and (g) also indicate a preferential alignment orthogonal to the substrate surface. Such an alignment is produced by the combination of the plasma sheath electric field perpendicular to the substrates and the increase of the rigidity of the nanofibers upon the formation of the $TiO_2$ shell. Taking a look in detail, it is evident from the metallic grid (Figure 1d–g) and cellulose filters (Figure 1h–k) the good conformality obtained with the plasma-assisted growth allowing the development of a high density of NFs over the all exposed geometrical features and inner parts of the 3D supports. Besides, it is also worth mentioning that the application of the plasma-assisted technology ensures good adhesion of the NFs to both rigid and soft substrates, which are

also chemically different. Thus, for the first time, we demonstrate that the soft-template approach combined with PECVD of $TiO_2$ carried out at room temperature allows the decoration of substrates with open porosity as the stainless steel membranes and highly temperature-sensitive materials like the cellulose filters.

### 2.2. Wettability of the 3D Nanomembranes

The first step toward the development of wetting tunable surfaces is the characterization of static and dynamic contact angles to liquids with different polarities. **Table 1** summarizes such characteristics for the different materials developed in this work giving emphasis on the comparison of NFs fabricated on flat and 3D supports and the wetting character toward water (polar) and diiodomethane (nonpolar) drops. The dynamic properties, i.e., rolling-off angle (RoA), are presented for the samples with a marked hydrophobic and/or oleophobic character.

The reference silicon and fused silica substrates are both hydrophilic and oleophilic given the low contact angle values listed in Table 1. However, the surface functionalization of them with $H_2Pc@TiO_2$ NFs results in a pronounced increment in the water contact angle (WCA) reaching values as high as 134° and 123°, respectively. On the contrary, the diiodomethane contact angle (DCA) is decreased indicating an enhanced oleophilic surface state of the fused Si and Si substrates. In the case of the porous membranes, the starting wettability is quite different from the reference materials, whereas cellulose appears completely superhydrophilic and superoleophilic; the metallic grid presents high contact angle values with both polar and nonpolar liquid droplets. When the $H_2Pc@TiO_2$ NFs are formed onto the cellulose, the wetting changes from being a completely water-permeable membrane to prevent water absorption regardless of the pore size tested (**Figure 2**a,b; see also Video S1 in the Supporting Information). For the metallic grid, the hydrophobicity is improved upon the formation of the NFs reaching a full water droplet repellence level (Figure 2c,d), at the same time that the membrane goes from oleophobic (85°) to oleophilic (34°). The decorated cellulose keeps its high surface tension when put in contact with droplets of low-tension liquids (see Table 1). This experience confirms the transition of the wetting behavior from Wenzel-like to Cassie–Baxter-like surfaces[22] when combining three roughness levels, from the several tens of micrometers of the porous substrates to the micrometer length of the nanofibers and the nanoscale morphology of the $TiO_2$ shell formed by plasma-enhanced chemical vapor deposition. In this way, the decoration of the commercial membranes with the $H_2Pc@TiO_2$ NFs without further bulk chemical and physical modifications, whether metallic or cellulose, provides them with a selective superhydrophobic and superoleophilic wetting.

Sliding tests were also carried out for the highly hydrophobic samples (see Table 1). For such characterization, the droplets are deposited onto the surface, and then the whole system is tilted until the drop rolls off. The bare metallic filters depict a petal effect behavior,[23] i.e., even for high WCAs, there is no sliding. Once the filters are decorated with the NFs, the surface presents sliding angles compatible with the lotus effect (RoA ≈ 10°),[24] showing a low adhesion against water droplets' impact. These values are smaller than that presented by the nanostructured flat references (RoA ≈ 20°). The lowest sliding angles have been found from the $H_2Pc@TiO_2$ NFs on the cellulose membranes, even indicating a lack of adhesion of 10 µL water droplets when they fall on the lower-porous-size cellulose substrate. Therefore, the surface functionalization of porous materials employing nanostructures with a high aspect ratio, the so-called 3D nanomembranes, has allowed the acquisition of a superhydrophobic capacity together with a superoleophilic response. Such characteristics can be exploited to select the liquids passing through the nanomembranes and for the separation of liquid mixtures mainly with water and, consequently, in controlling the direction of movement of a fluid.

The stability of the NF nanomembranes depends on several factors such as the composition of the fibers, mechanical or chemical stability upon contact with the liquid drops, and adhesion of the fibers to the support. In our case, the $TiO_2$ composition of the shell endows the NFs of high chemical and thermal stability at the same time that the organic core provides flexibility to accommodate the impact and movement of the drops on the nanomembrane surface. On the other hand, the PECVD methods are widely applied to the conformal deposition of metal oxides and polymers on supports of an ample variety of compositions and shapes given their enhanced performance from the point of view of surface tension adjustment and compatibility with intermediate layers to improve the adhesion of the growing material. Thus, the critical issues in our system are the role played by the substrate itself, particularly dealing with the hygroscopic cellulose, and the integrity of the NFs after repeated cycling of wetting with polar and nonpolar liquids. In this regard, **Figure 3** shows SEM images corresponding to the nanostructured cellulose surface after leaving

**Table 1.** Values of water and diiodomethane contact angles (WCA and DCA, respectively) and rolling-off angles (RoA) with water (W-) and diiodomethane (D-) droplets for $H_2Pc@TiO_2$ NFs deposited onto porous membranes and smooth compact reference substrates for comparison.

| Sample | WCA [°] | W-RoA [°] | DCA [°] | D-RoA [°] |
|---|---|---|---|---|
| Fused Si | 24 | >90 | 19 | – |
| Si | 27 | >90 | 10 | – |
| 11 µm cellulose | 0 | – | 0 | – |
| 25 µm cellulose | 0 | – | 0 | – |
| Metal grid | 133 | >90 | 85 | >90 |
| $H_2Pc@TiO_2$ NFs on fused Si | 134 | 20 | 0 | – |
| $H_2Pc@TiO_2$ NFs on Si | 123 | 25 | 0 | – |
| $H_2Pc@TiO_2$ NFs on 11 µm cellulose | ≈180 | 0 | 0 | – |
| $H_2Pc@TiO_2$ NFs on 25 µm cellulose | ≈180 | 17 | 0 | – |
| $H_2Pc@TiO_2$ NFs on metal grid | ≈180 | 10 | 34 | – |
| $H_2Pc@TiO_2$ + F-grafting NFs on metal grid | ≈180 | 5 | 153 | 35 |
| $H_2Pc@TiO_2$ + PDMS + F-grafting NFs on metal grid | ≈180 | 5 | 136 | 15 |

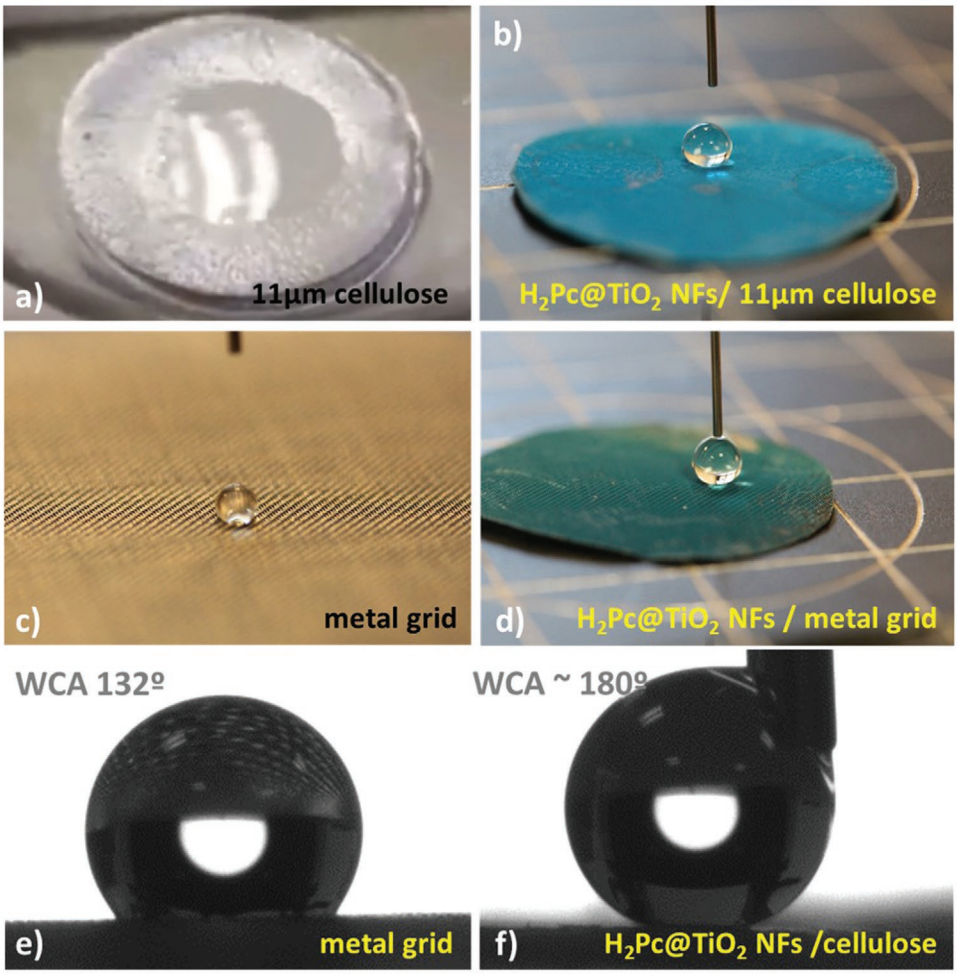


**Figure 2.** Superhydrophobic cellulose and metal grid. Wetting behavior of the cellulose filter and metallic grid a,c) before and b,d) after the decoration with the $H_2Pc@TiO_2$ NFs. Droplets of 10 µL were used in panels (b) and (d) (even with the tip inside) due to the high repellency of the surface to get a static configuration. e,f) Water contact angle images of 2 µL droplets deposited on the metal grid and the $H_2Pc@TiO_2$ NFs/cellulose surfaces, respectively. (In this last, the tip was kept inside trying to counteract capillarity effects versus surface repellency.)

a large water droplet on it for 10 min. Microstructural changes such as dilation and/or smoothing effects are evident. However, 3D nanostructure remains attached to the surface of the cellulose as a proof of the NFs' stability even after several cycles of contact with water and diiodomethane. Anyway, in Section 2.5 we will discuss again this matter and propose the use of PDMS embedding to further improve the mechanical stability of the NFs.

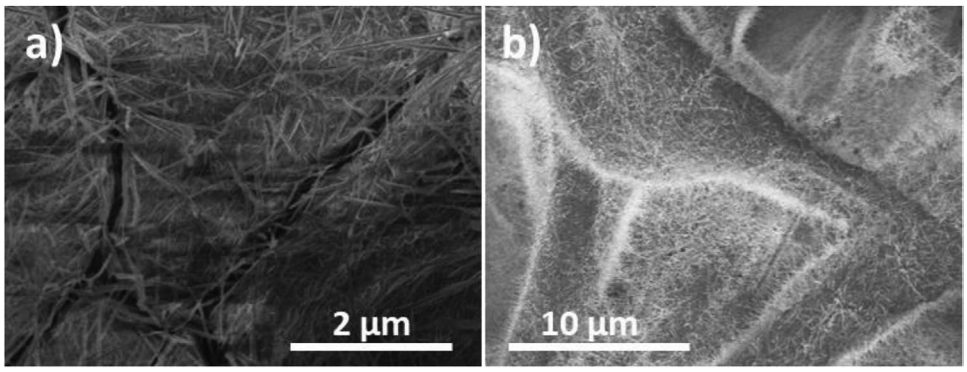


**Figure 3.** The NFs remain stable on cellulose after contact with water drops. Hygroscopic effect on the cellulose a) 11 µm and b) 25 µm pore-size filters decorated with the $H_2Pc@TiO_2$ NFs just after wetted with water droplets of 3 µL volume for 10 min.

### 2.3. Liquid Filtration and Selectivity Capacity of 3D Nanomembranes' Evaluation

To demonstrate the application of the superhydrophobic/superoleophilic wetting behavior of the nanomembranes for liquid filtration, we settled the experiment shown in **Figure 4** (see also "Experimental Section" and also Video S2 in the Supporting Information). The panels compare the results of a) the metallic grid, b) 25 µm, and c) 11 µm cellulose filters decorated with $H_2Pc@TiO_2$ NFs upon a liquid filtration/separation test with a 1:1 emulsion of the two liquids, water and diiodomethane, with a constant flux controlled by a syringe. As it is visible in the photographs and Video S2 (Supporting Information), the accumulated droplets from the emulsion mostly seem to expand over the surface although there is some liquid remaining with a semispherical shape onto it. This phenomenon responds to the lower surface tension reaction of water in the first stages of the experiment (Figure 4a-1,b-1,c-1). Meanwhile, the higher density and surface tension of the nonpolar liquid produce an immediate spreading of the diiodomethane onto the whole surface. Such a behavior is more pronounced for the cellulose filters as depicted in Figure 4b-2,c-2). As the number of drops increases, they begin to coalesce forming a macrodroplet with an increasing size until the entire surface is covered (Figure 4a-3,b-3,c-3). At this stage, the diiodomethane is separated from water through the modified membranes thanks to the combination of gravity and the superhydrophobic/superoleophilic character of the 3D nanomembrane surfaces. Moreover, it is important to stress herein that no color changes were observed either in the filtered diiodomethane or in the isolated water resulting from a hypothetical detachment or dilution of the nanofibers. Thus, the diiodomethane coming from the emulsion is successfully collected from the bottom of the flask leaving clean, uncolored, and odorless water drops on the top side of the membranes (Figure 4a4–c4).

### 2.4. Photoactivation of 3D Nanomembranes for a Selective Control Wetting

A great advantage of the methodology applied for the formation of the core@shell nanofibers is that it opens the path to develop multifunctional systems by either combining materials

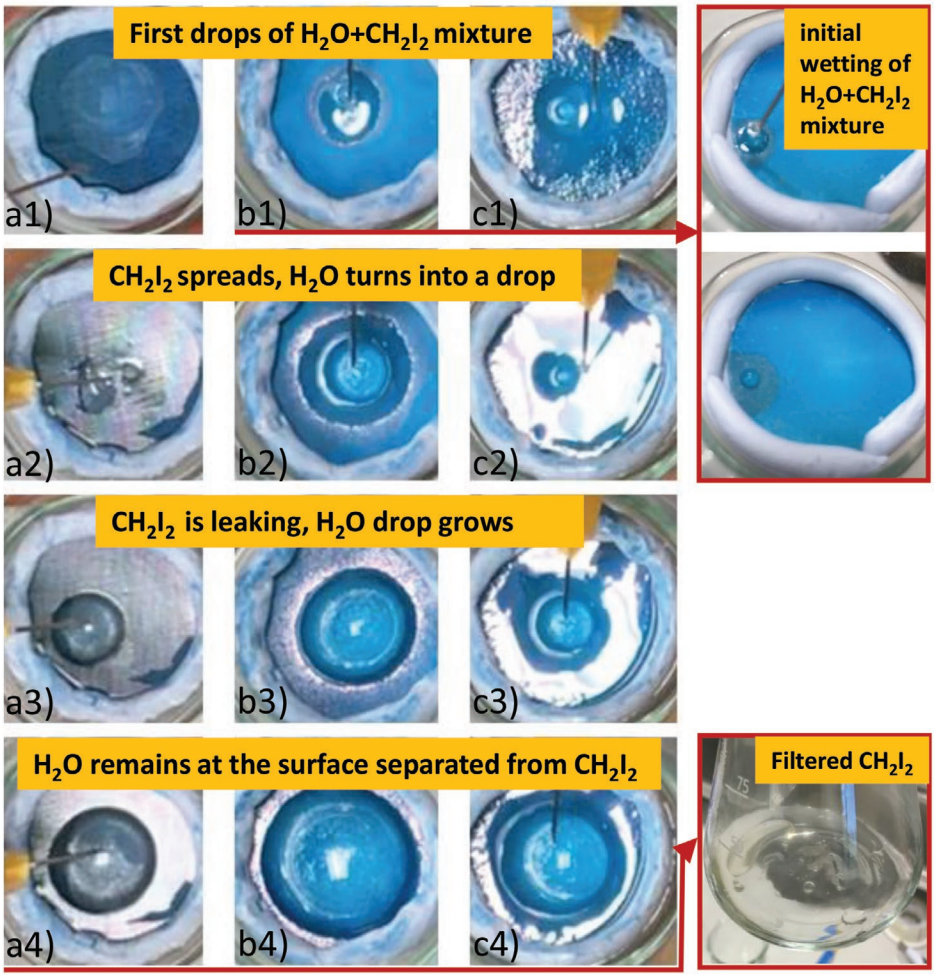


**Figure 4.** Nonpolar/polar liquid filtration and separation. The photographs show the filtration sequences of a 1:1 diiodomethane/water emulsion by the nanomembranes of a) metal grid and cellulose filter of b) 25 µm and c) 11 µm decorated with $H_2Pc@TiO_2$ NFs. Water remains on the surface and diiodomethane leaks out as a result of the superhydrophobicity and superoleophilicity of these 3D nanomembrane surfaces (see also Video S2 in the Supporting Information).

with different functionalities on the nanoarchitecture or by taking advantage of the multifunctional character of the material forming the shells. In the previous section, we have indicated how the inert chemical character of the $TiO_2$ together with the mechanical properties of the organic core improves the stability of the nanomembranes. Here, we will profit from the photoactive response of the $TiO_2$ shells to allow the reversible superhydrophobic-to-superhydrophilic conversion upon illumination with UV light.[25,26] The graphs in **Figure 5** present the evolution of the 3D nanomembrane's contact angle to water under a) visible (Vis) and b) UV–vis illumination. Interestingly, the water contact angle of the surfaces fabricated on cellulose and metallic grids is decreased after the first minutes of illumination with Vis light, and an unexpected result as the $TiO_2$ presents photoactivity under excitation at UV wavelengths. Thus, there is a parallel decrease in WCA of about 20° for both types of samples after illumination during ≈200 s. Afterward, the WCA is extremely stable, independently of the duration of the exposition keeping its superhydrophobic character. Such a result might be related to the light absorption capability of these substrates[27,28] as the sample fabricated on the Si(100) shows a completely stable response. The situation strongly differs from the illumination with UV–vis wavelengths that produces a fast conversion of the three surfaces into hydrophilic. However, the behavior depends on the type of support, as on the metallic grid the WCA decreases slower than for the silicon and cellulose. It is only on the cellulose filter where the conversion is completed within the time lapse of the experiment, becoming superhydrophilic after 600 s of illumination. Other hydrophobic membranes decorated with $TiO_2$ nanoparticles have revealed slower photoactivation[29] or needed high synthesis temperature protocols.[30] Mechanisms of water condensation onto hydrophilic or hydrophobic $TiO_2$ thin films and highly porous nanostructures have been previously studied[26,31,32] to control precisely the photoactivation of wettability. As also reported for other photoactive, low-dimensional metal oxide nanomaterials, the superhydrophobic character of the surfaces can be recovered by heating, dark storage during a few weeks, or in a low vacuum overnight.[33–37] These results open the path for the use of the $TiO_2$ nanomembranes as photonic microfluidic valves for the selection of liquids under light activation and as self-cleaning membranes or sensors, which can be further used for photocatalytic removal of water pollutants.[38]

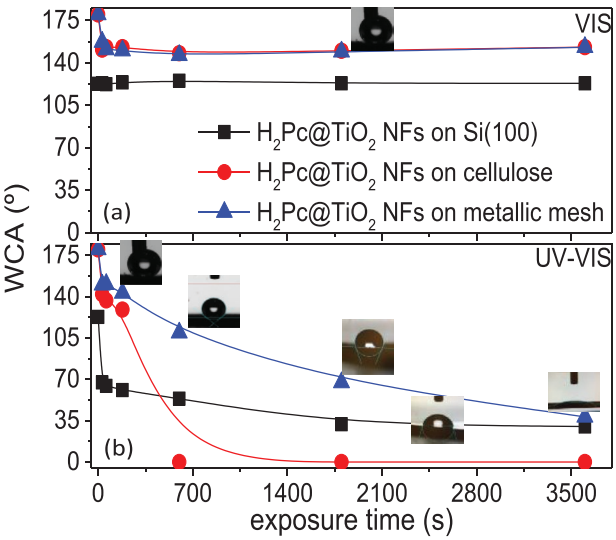


**Figure 5.** Superhydrophobic-to-superhydrophilic conversion, the effect of the irradiation wavelength, and support. Variation of the contact angle with the irradiation time of the nanomembrane on the metallic grid, 11 µm cellulose filter, and Si reference substrate as labeled under a) visible and b) UV–vis illuminations.

### 2.5. Omniphobic $H_2Pc@TiO_2$ 3D Membranes after Fluorine Surface Functionalization

In this section, we will show how to modify the 3D nanomembranes to fabricate superomniphobic surfaces by chemical modification of the $TiO_2$ shells by molecular grafting of fluorinated silanes. The method involves the exposure of the $H_2Pc@TiO_2$ NFs to soft oxygen plasma to ensure a highly reactive surface to prompt the chemical bonding through the Si— in the perfluorooctyltriethoxysilane (PFOTES) to the —OH groups on the metal oxide shell surface (see the "Experimental Section" and ref. [39]). The use of the oxygen plasma pretreatment provides environmentally friendlier conditioning of the metal oxide surface, in comparison with the standardized refluxing in solvents like toluene[40] and enhances the compatibility of the grafting with hygroscopic substrates as the cellulose. The F-grafting reduces the rolling-off angle to water as shown in the photographs in **Figure 6**a, where a 1 µL water droplet bounces three times on the surface before being ejected for F-grafted NF-decorated metallic grid in a flat position. Meanwhile, 10 µL water droplets slide under tilted angles of around 5° as is reported in Table 1. Such surface functionalization strongly affects the contact angle to nonpolar liquids as gathered in Table 1 with a DCA as high as 153° and rolling-off-angles below 35° for 5 µL diiodomethane droplets. Previous results of alternative surface fluorine-based membranes fabricated with polymers[41] or graphene oxide[42] (applied on ion exchange) have been reported but involved complex wet chemical routes to reach only a hydrophobic state. However, omniphobic polymeric membranes for distillation[43,44] found in the literature are neither fully water repellent nor slippery. Moreover, attending to the approaches based on the nanostructuration of membranes with nanoparticles,[45,46] the omniphobicity has only linked to sliding capacity against water droplets.

In a further step to enhance the omniphobicity, the NFs were embedded in a highly flexible polymer, PDMS. This approach has been previously reported to improve not only the contact angle to nonpolar liquids but also to delay the formation of ice on the surface of high-aspect-ratio nanostructured materials.[47] Moreover, the embedding on a stretchable polymer is also expected to improve the adhesion of the NFs, mechanical stability, and flexibility of the nanomembranes. Thus, the $H_2Pc@TiO_2$ NFs were covered with a thin layer of PDMS (see the "Experimental Section") and later subjected to the F-grafting. **Figure 7**a–c presents characteristics SEM images of the NF-decorated metallic grid after the PDMS deposition. Several aspects may be stressed at this point: first, panel (a) and energy dispersive X-ray (EDX) spectroscopy analysis in panels (d)–(i) show that the PDMS coating process does not clog the membrane pores

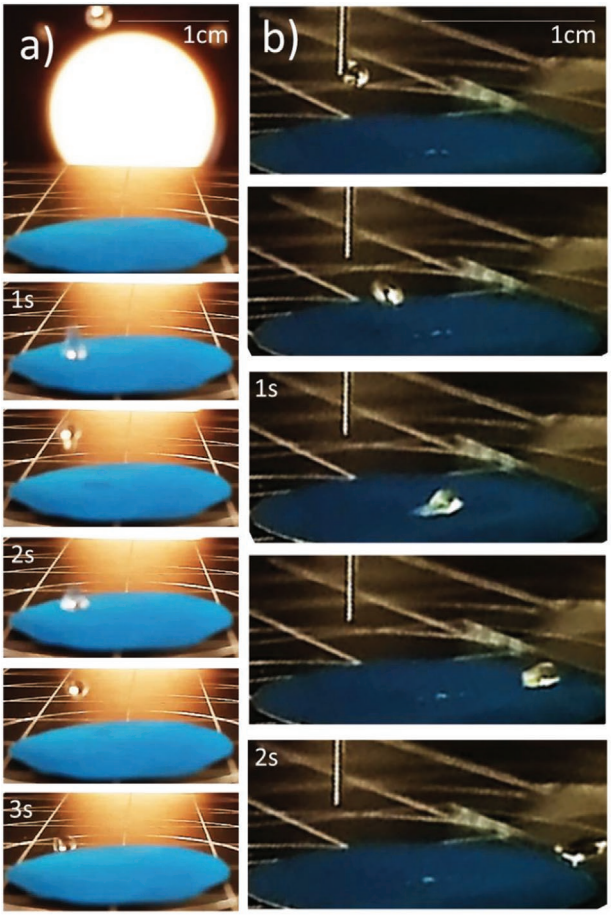


**Figure 6.** Superomniphobicity of F-grafted and F-grafted/PDMS nanomembranes. a) Pictures of 1 µL water droplet repellence of the F-grafted $H_2Pc@TiO_2$ NFs on the metallic grid. b) Pictures of 1 µL diiodomethane droplet sliding and repellence of the PDMS/F-grafted $H_2Pc@TiO_2$ NFs on the metallic grid tilted 5°. (Pictures taken from videos recording at 240 fps). Please note that the focus is settled when the drop is yet pinning to the needle.

of the metallic grid. This is an important result, as it implicates that the embedding in the polymer does not alter the filtering capacity of the grid to air or gases (as it is demonstrated in Video S3 in the Supporting Information). Second, although part of the NFs appear completely buried in the polymer, yet the microscale roughness of the surface is high, as the heads of the longest NFs stand out of the PDMS surface. Indeed, this effect reduces the overall solid area fraction, even in comparison with the as-grown NFs, which produce an improvement in the RoA for both polar and nonpolar liquids (see Table 1). As an example, Figure 6b shows how a 1 µL diiodomethane droplet falling on the tilted PDMS/F-grafted membrane freely moves out of it. Finally, it is worth mentioning that the long NFs are also conformally embedded by the polymer (Figure 7c). In this way, in the longest NFs, we can observe a hybrid system formed by a conformal PDMS layer that fills the pores and gaps at the surface of the metal oxide shells. A similar approach has recently been reported to enhance the performance of 1D nanomaterial layers regarding the mechanical robustness under bending, strain, and stress cycling such as for carbon nanotubes, ZnO, and Cu and Ag nanowires.[48–51] In the context of our work, it is expected that the formation of the hybrid $H_2Pc@TiO_2$/PDMS NFs improves the durability of the 3D nanomembranes as it enhances the flexibility, and robustness of the nanofiber under continuous drop impacts and, not only under mechanical stress, but also below UV and visible illumination for long periods.

To further visualize the superomniphobic behavior, **Figure 8** (see also Videos S4 and S5 in the Supporting Information) collects a series of images of the F-grafted nanomembrane when it is exposed to the 1:1 emulsion of water and diiodomethane. Panels (a1) and (a2) show how the liquid emulsion only filters at the edge between the membrane and the tube. Even small water droplets are observed rolling off from the surface and sticking to the outer wall of the tube (see Figure 8a1–a6). It should be noted that although diiodomethane presented some wetted surface area on the functionalized membrane, as the contact angle is ≈153°, the nonpolar liquid is not filtered through it and remains in the $H_2O + CH_2I_2$ mixture in a retained droplet of increasing volume. In the case of the PDMS/F-grafted NFs (Figure 8b1–b6), the liquid emulsion is retained onto the surface with a most evident liquid separation, and as the liquid volume increases, small droplets are detached rolling off the outer walls of the tube (Figure 8b6). It should be mentioned that during the experience time, diiodomethane remained on top of the membrane porous supporting even the gravitational action of the accumulated water above, and its higher density without being decanted to the bottom of the tube as a dominant surface tension effect, unlike what was observed in Figure 4. An additional advance of the surface functionalization and polymer embedding by this approach is its long-lasting character. Thus, it was proved that after 1 h of UV–vis irradiation the F-NFs, the WCA changed to 124° and the DCA to 136°, whereas the addition of PDMS and posterior fluorine grafting of the 3D membranes still depicted a superomniphobic character after 60 min of UV illumination.

### 2.6. Self-Cleaning Capability of Omniphobic $H_2Pc@TiO_2$ 3D Membranes

Besides the possibilities of selective liquids' separation or completely liquid repellence, the 3D nanomembranes can take advantage of their omniphobic character to develop self-cleaning properties not only toward polar and nonpolar liquids but also to solid pollutants. Unlike other self-cleaning methodologies relying on the application of external factors or agents[52,53] to the membranes, herein, we have carried out an autocleaning test by dosing water droplets on top of a 3D nanomembrane surface contaminated with graphite powder upon the dosing of water droplets. This simple test has been previously applied to show the self-cleaning properties against dust of superhydrophobic surfaces.[54–56] Different surface functionalization routes of the metallic grid have demonstrated dissimilar self-cleaning levels as it is shown in **Figure 9** and in Video S6 (Supporting Information). $H_2Pc@TiO_2$ NFs' surface can remove the dirt accumulated on it upon water droplets impact. Since these surfaces, although superhydrophobic, have a higher rolling-of angle, water droplets of increasing volume remain on the surface containing graphite powder particles inside and

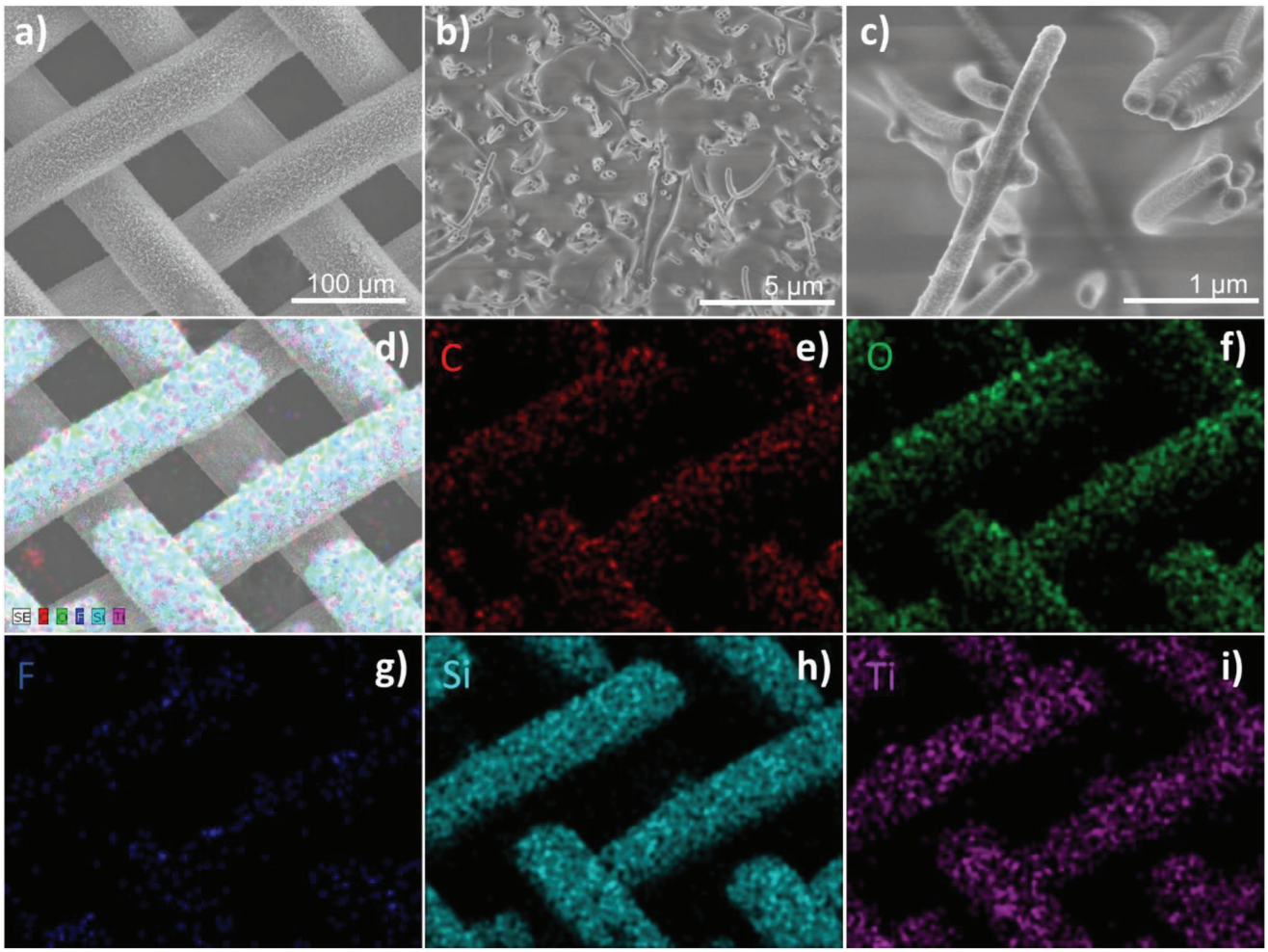


**Figure 7.** Embedding the $H_2Pc@TiO_2$ NFs nanomembranes in a stretchable polymer matrix. a–c) SEM images at different magnifications after the F-grafting and PDMS modification of the metallic grid decorated with NFs. d) EDX combined and e–i) elemental signals' images for the different elements as labeled of the PDMS/F-grafted $H_2Pc@TiO_2$ NFs on the metal grid.

floating on its surface until a certain volume when the droplet is detached from the 3D nanomembrane (Figure 9a). Similar performance presented the F-grafted NFs on the metallic grid but in a faster self-cleaning way; this surface needed droplets of smaller volume to drag clearer dirt off the surface. When the PDMS/F-grafted NFs on the metallic grid are subjected to the self-cleaning test, it is observed in Figure 9c and Video S6 (Supporting Information) the complete removal of dirt already from

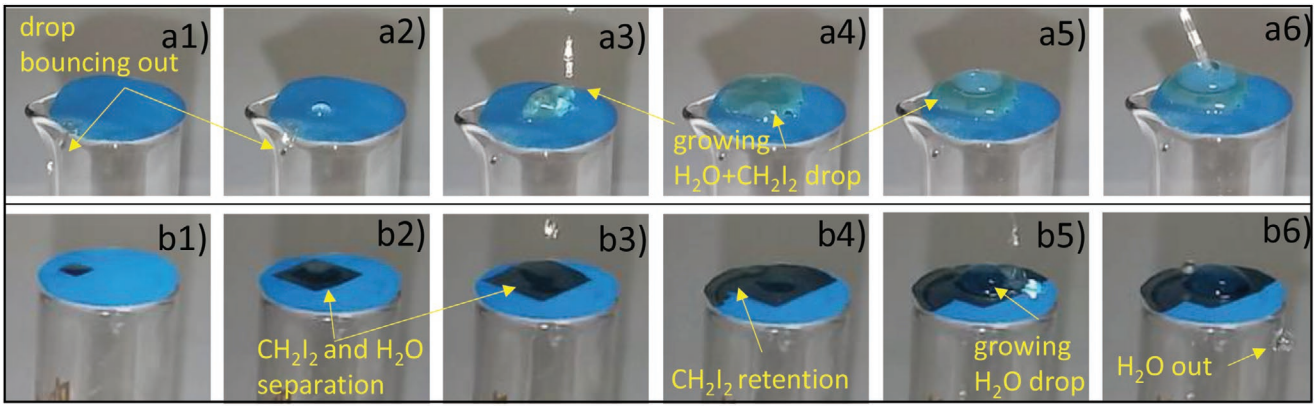


**Figure 8.** Stability of the omniphobic 3D nanomembrane. Pictures of the 3D nanomembranes on metallic grid in contact with a 1:1 water/diiodomethane emulsion, functionalized with a) F-grafted $H_2Pc@TiO_2$ NFs, b) PDMS/F-grafted $H_2Pc@TiO_2$ NFs after being UV–vis irradiated.

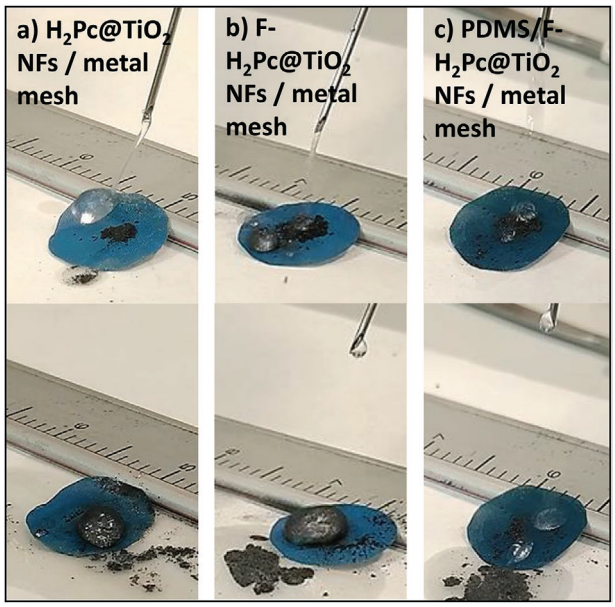


**Figure 9.** Self-cleaning omniphobic 3D nanomembranes. Pictures of the self-cleaning response of the carbon dirty 3D nanomembranes on the metallic grid under the impact of water droplets, functionalized with a) $H_2Pc@TiO_2$ NFs, b) F-grafted $H_2Pc@TiO_2$ NFs, and c) PDMS/F-grafted $H_2Pc@TiO_2$ NFs.

the first small drops sliding on the surface and removing the graphite along the path they travel. Such phenomenology is in good agreement with the results in Table 1, showing the lower RoA and, therefore, lower adhesion for the hybrid PDMS/F-grafted H2Pc@$TiO_2$ NFs' membrane, where water drops push and drag the polluting particles.

Outstandingly, the PDMS/F-grafted modified nanomembranes presented self-cleaning properties even for very small dirt particles.[57] Thus, Figure S1 (Supporting Information) gathers SEM images taken at different magnifications showing the completely clean and bare 3D nanomembranes after the water droplets' impact. In the case of membranes, autocleaning supposes a highly desirable property when dust particles precipitate and new fluid pollutants can be present in liquids or liquid mixtures during separation and filtration performances.

## 3. Conclusion

In this work, we have expanded the organic nanowires' soft-template method for the development of core@shell nanowires and nanofibers to the fabrication of 3D nanomembranes. The application of PECVD for the formation of metal oxides, such as amorphous $TiO_2$, has provided a reliable way to grow both the seed layers and the nanofibers shells. At the same time, we have demonstrated the compatibility of the method with the surface modification of complex 3D supports of different chemical nature as metal grides and cellulose filters working under room temperature conditions. The nanofibers formed by this protocol show 3D shells endowed with nanoscale roughness, concretely, presenting a cauliflower-like morphology. This has produced a triple scale of roughness, including the microscale length of the fibers (in the order of micrometers) and the characteristic morphology of the porous supports (tens of micrometers), bringing up a marked superhydrophobic behavior including on the hygroscopic cellulose filters. We have taken advantages of the oleophilic character of the $TiO_2$ to fabricate membranes for the separation of polar and nonpolar liquids, showing, in addition, its photoactivity under visible and UV illuminations. Thus, the membranes become hydrophilic after illumination with UV light for less than 1 h. The oxygen-plasma-mediated grafting approach has allowed us the functionalization of the membranes with fluorinated molecules even on hygroscopic substrates such as cellulose. In this way, superomniphobic surfaces have been developed and demonstrated with self-cleaning capacity. F-grafting combined with PDMS embedding of the nanofibers has resulted in the highest performance functionalization allowing for self-cleaning properties against small dirt particles, keeping these properties after long exposition to air conditions, including also UV illumination. However, this functionalization does not clog the metal grid holes, letting air and gases passing through. Therefore, we are presenting a surface technology that can not only discriminate liquids by surface tension but also distinguish between fluid phases.

## 4. Experimental Section

*Materials*: 3D nanostructures were deposited on porous supports and reference compact and smooth substrates, such as Si (100) silicon and fused silica of $1.5 \times 1.5$ $cm^2$. Commercial membranes used as substrates for the 3D nanostructure decoration were S0770 SS grid filter from Sigma–Aldrich, with 40 mm diameter and 70 µm pore size, employed to treat water with suspended pollutants in stages before flexible filters; Whatman qualitative cellulose filter, grade 1, of 42.5 mm diameter and 11 µm pore size, used on low flow retention filtration processes and liquid clarification commonly applied in soil and seed analyses, drying food, or atmospheric gas control; and Whatman qualitative cellulose filter, grade 4, of 40 mm diameter and 25 µm pore size, commonly used in filtration processes as that of grade 1.

*3D Nanomembrane Fabrication*: The $TiO_2$ nanofibers were fabricated by a soft-template approach based on the deposition of single-crystalline ONWs as 1D templates. Scheme 1 shows the main steps in the synthesis of the nanofibers. The methodology for the formation of the $TiO_2$ nanofibers involves three basic steps: step 1—deposition of the nucleation centers on flat substrates and porous supports; in this case, a nanoporous $TiO_2$ layer was deposited by PECVD. Characteristic SEM images are gathered in Scheme 1a,b showing a high conformality of the $TiO_2$ layer depicting the typical cauliflower morphology corresponding to the formation at room temperature under 100% oxygen plasma.[58] Step 2: The driven mechanism for the formation of the organic nanowires is a crystallization process led by the high directionality of the self-assembly of the organic molecules by $\pi$-stacking; additional details on such a synthetic procedure can be found elsewhere.[21,59] Simple thermal evaporation, i.e., a physical vapor deposition (PVD) was applied under mild temperature and vacuum conditions for the formation of $H_2Pc$) nanowires. The growth conditions such as substrate temperature, growth rate, deposition duration, and size of the nucleation sites determine the density, shape, and length of the organic nanowires. Thus, Scheme 1c,d shows the variation in the density of the nanowires for the deposition under two different growth rates namely c) <0.5 Å $s^{-1}$ and d) >1.5 Å $s^{-1}$ of $H_2Pc$ nanowires formed on a $TiO_2$ nucleation layer. Step 3: The last step consists of the deposition of an organic or inorganic shell by plasma-assisted deposition methods[60] forming a core@shell nanowire or nanofiber, where the core is formed by the organic nanowire, and the shell conformally covers the core giving rise to a hierarchical

nanomaterial where the shell keeps its particular microstructure and properties. The thickness of the shell is easily tunable by controlling the deposition time. The core can be removed by annealing at a mild temperature;[60] however, the results in this article corresponded to the core@shell nanostructures labeled herein as $H_2Pc@TiO_2$ NFs. The presence of the core is the reason why the cellulose and metal grids appear blue in color, as a consequence of the typical *Q*-band absorption characteristic of these organic functional molecules.[61] Step 4: Scheme 1 addresses the repetition of steps 1–3 on both sides of the 3D supports.

For steps 1 and 3, nanoporous $TiO_2$ coatings of 200 nm thickness were grown by PECVD at low pressure under cyclotron electron resonance working at 2.45 GHz (electron cyclotron resonance microwave (ERC MW)) conditions from a volatile titanium tetraisopropoxide (TTIP) precursor: deposition time of 1 h, applied a power of 68.0 W, and oxygen as gas plasma at $9 \times 10^{-3}$ mbar were the experimental conditions. The selected molecule for the formation of NFs was 29*H*,31$H_2$Pc purchased from Sigma–Aldrich. The molecules were sublimated without further purification at $2 \times 10^{-2}$ mbar of Ar for a substrate temperature of 170 °C, and a growth rate of 1 Å $s^{-1}$ (estimated by a quartz crystal microbalance emplaced at the same distance as the substrates) for 1 h. The synthesis of the $H_2Pc@TiO_2$ fibers was reproduced on both sides of the cellulose and stainless steel membranes under the same experimental conditions.

*Surface Functionalization*: Fluorine-based grafting was based on the chemical derivatization of the oxide surface by the reaction of surface —OH groups with a perfluorinated silane. For this purpose, the surface of the $TiO_2$ nanofibers was exposed to 1*H*,1*H*,2*H*,2*H*-PFOTES vapor kept in a thermal bath at 80 °C during 3 h after a previous vacuum pump.[39] The samples surfaces were preactivated at the same MW ECR reactor used for the PECVD for 10 min at an oxygen pressure of $4 \times 10^{-2}$ mbar and 700 W. Moreover, to provide mechanical robustness to the nanofibers, 3D nanomembranes were coated with a PDMS thin film (2:1 of PDMS precursor and curing agent from Sylgard) in a 1:3 toluene solution employed in a spin-coating system. Finally, these PDMS-embedded 3D nanomembranes were also exposed to the fluorine-based grafting.

*Characterization of 3D Nanomembranes*: SEM images were acquired in a Hitachi S4800 working at 2 kV both in reference substrates and commercial membranes. The statistical analysis of the nanofibers morphology and density was mainly carried out by inspection of microscopic images taken at different magnifications. The wettability was evaluated, after 1 week of sample storage, through liquid droplet contact angle measurements with polar (Milli-Q water, WCA) and nonpolar ($CH_2I_2$ diiodomethane, DCA) by the static sessile drop method in an OCA20 from DataPhysics Instruments GmbH. Drops of 1 µL were deposited onto the surface for static measurements, whereas 10 and 5 µL were used for sliding/RoA analysis with water and $CH_2I_2$, respectively. It should be noted that on hydrophilic surfaces the RoA measurement was not possible. Statistics over five drops on each surface were presented as a mean contact angle value with estimated errors between 3% and 7%. Finally, the surface was photoactivated by UV irradiation in air, under ambient conditions, with the full spectrum of a 175 W ASB-XE-175 xenon fiber optic light source lamp. The study of the separation capacity of a water–diiodomethane emulsion was carried out in a homemade device consisted of a glass funnel and a sealant material to support nanomembranes of 19 mm diameter and to avoid liquid leaks.

## Supporting Information

Supporting Information is available from the Wiley Online Library or from the author.

## Acknowledgements

The authors thank the AEI-MICINN (PID2019-110430GB-C21 and PID2019-109603RA-I0), the Consejería de Economía, Conocimiento, Empresas y Universidad de la Junta de Andalucía (PAIDI-2020 through projects US-1263142, ref. AT17-6079, P18-RT-3480), and the EU through cohesion fund and FEDER 2014–2020 programs for financial support. C.L.-S. and J.R.S.-V. thank the University of Seville through the VI PPIT-US and (J.R.S.-V.) the Ramon y Cajal Spanish National programs. The projects leading to this article received funding from the EU H2020 program under the grant agreements 851929 (ERC Starting Grant 3DScavengers) and 899352 (FETOPEN-01-2018-2019-2020—SOUNDofICE).

## Conflict of Interest

The authors declare no conflict of interest.

## Data Availability Statement

Research data are not shared.

## Keywords

nanofibers, plasma deposition, self-cleaning surfaces, superomniphobicity, tunable wetting

Received: May 12, 2021
Revised: June 24, 2021
Published online: October 7, 2021

[1] https://ec.europa.eu/environment/water/quantity/scarcity_en.htm (accessed: May 2021).
[2] M. A. Hassaan, A. El Nermr, *Egypt. J. Aquat. Res.* **2020**, *46*, 207.
[3] V. Geissen, H. Mol, E. Klumpp, G. Umlauf, M. Nadal, M. Van Der Ploeg, S. Van Der Zee, C. J. Ritsema, *Int. Soil Water Conserv. Res.* **2015**, *3*, 57.
[4] T. A. Saleh, V. K. Gupta, *Nanomaterial and Polymer Membranes: Synthesis, Characterization, and Applications*, 1st ed., Elsevier, Amsterdam, The Netherlands **2016**.
[5] E. N. Peleka, K. A. Matis, *Ind. Eng. Chem. Res.* **2011**, *50*, 421.
[6] Z. Zhang, M. J. Qi, Y. F. Qian, R. Y. Song, B. Du, *Therm. Sci.* **2015**, *19*, 1267.
[7] C. M. Modise, J. A. Bendick, C. J. Miller, R. D. Neufeld, R. D. Vidic, *Water Environ. Res.* **2006**, *78*, 557.
[8] S. Judd, B. Jefferson, *Membranes for Industrial Wastewater Recovery and Re-Use*, 1st ed., Elsevier, Amsterdam, The Netherlands **2003**.
[9] A. K. Pabby, S. S. H. Rizvi, A. M. S. Requena, in *Handbook of Membrane Separations: Chemical, Pharmaceutical, Food, and Biotechnological Applications*, 2nd ed., CRC Press **2020**.
[10] R. Molinari, C. Lavorato, P. Argurio, *Membranes* **2020**, *10*, 281.
[11] R. W. Baker, *Membrane Technology and Applications*, John Wiley & Sons Ltd, Chichester, West Sussex, UK **2004**.
[12] P. Sajeesh, A. K. Sen, *Microfluid. Nanofluid.* **2014**, *17*, 1.
[13] Z. Wang, D. Hou, S. Lin, *Environ. Sci. Technol.* **2016**, *50*, 3866.
[14] A. K. Kota, G. Kwon, W. Choi, J. M. Mabry, A. Tuteja, *Nat. Commun.* **2012**, *3*, 1025.
[15] X. Lu, W. Si, X. Sun, B. Liu, L. Zhang, C. Yan, O. G. Schmidt, *Nano Energy* **2016**, *19*, 428.
[16] J. D. Winans, J. J. P. Smith, T. Gaborski, J. L. Mcgrath, *J. Membr. Sci.* **2015**, *499*, 282.
[17] Z. Ma, G. Qin, in *Semiconductor Nanomaterials for Flexible Technologies: From Photovoltaics and Electronics to Sensors and Energy Storage*, (Eds: Y. Sun, J. A. Rogers), Elsevier, Amsterdam, The Netherlands **2010**, p. 67. ISBN: 9781437778243.
[18] H. Zhou, J. H. Seo, D. M. Paskiewicz, Y. Zhu, G. K. Celler, P. M. Voyles, W. Zhou, M. G. Lagally, Z. Ma, *Sci. Rep.* **2013**, *3*, 1291.

[19] L. Yao, J. He, *Prog. Mater. Sci.* **2014**, *61*, 94.
[20] E. L. Tian, H. Zhou, Y. W. Ren, Z. Mirza, X. Z. Wang, S. W. Xiong, *Desalination* **2014**, *347*, 207.
[21] M. Macias-Montero, A. N. Filippin, Z. Saghi, F. J. Aparicio, A. Barranco, J. P. Espinos, F. Frutos, A. R. Gonzalez-Elipe, A. Borras, *Adv. Funct. Mater.* **2013**, *23*, 5981.
[22] D. Murakami, H. Jinnai, A. Takahara, *Langmuir* **2014**, *30*, 2061.
[23] L. Feng, Y. Zhang, J. Xi, Y. Zhu, N. Wang, F. Xia, L. Jiang, *Langmuir* **2008**, *24*, 4114.
[24] B. Bhushan, M. Nosonovsky, *Encyclopedia of Nanotechnology*, Springer, Dordrecht **2012**.
[25] M. Macias-Montero, A. Borras, R. Alvarez, A. R. Gonzalez-Elipe, *Langmuir* **2012**, *28*, 15047.
[26] M. Macias-Montero, C. Lopez-Santos, A. N. Filippin, V. J. Rico, J. P. Espinos, J. Fraxedas, V. Perez-Dieste, C. Escudero, A. R. Gonzalez-Elipe, A. Borras, *Langmuir* **2017**, *33*, 6449.
[27] H. O. A. Hokkanen, I. Leppänen, K. Kammiovirta, M. Kapulainen, A. Harlin, *Cellulose* **2020**, *27*, 1543.
[28] M. A. Taher, S. Ponnan, H. Prasad, D. N. Rao, S. R. G. Naraharisetty, *Nanotechnology* **2020**, *24*, 175301.
[29] K. Fischer, M. Grimm, J. Meyers, C. Dietrich, R. Gläser, A. Schulze, *J. Membr. Sci.* **2015**, *478*, 49.
[30] M. J. Nalbandian, K. E. Greenstein, D. Shuai, M. Zhang, Y.-H. Choa, G. F. Parkin, N. V. Myung, D. M. Cwiertny, *Environ. Sci. Technol.* **2015**, *49*, 1654.
[31] A. Borras, C. Lopez, V. Rico, F. Gracia, A. R. Gonzalez-Elipe, E. Richter, G. Battiston, R. Gerbasi, N. McSporran, G. Sauthier, E. György, A. Figueras, *J. Phys. Chem. C* **2007**, *111*, 1801.
[32] V. J. Rico, C. López, A. I. Borrás, J. P. Espinós, A. R. González-Elipe, *Sol. Energy Mater. Sol. Cells* **2006**, *90*, 2944.
[33] F. H. Rajab, P. Korshed, Z. Liu, T. Wang, L. Li, *Appl. Surf. Sci.* **2019**, *469*, 593.
[34] J. Li, Q. Sun, S. Han, J. Wang, Z. Wang, C. Jin, *Prog. Org. Coat.* **2015**, *87*, 155.
[35] G. Caputo, R. Cingolani, P. D. Cozzoli, A. Athanassiou, *Phys. Chem. Chem. Phys.* **2009**, *11*, 3692.
[36] V. E. Vrakatseli, E. Amanatides, D. Mataras, *J. Phys.: Conf. Ser.* **2015**, *700*, 012039.
[37] Q. F. Xu, Y. Liu, F.-J. Lin, B. Mondal, A. M. Lyons, *ACS Appl. Mater. Interfaces* **2013**, *5*, 8915.
[38] A. N. Filippin, J. Castillo-Seoane, C. López-Santos, C. Rojas, K. Ostrikov, A. Barranco, J. R. Sánchez-Valencia, A. Borras, *ACS Appl. Mater. Interfaces* **2020**, *12*, 50721.
[39] V. Rico, J. Mora, P. García, A. Agüero, A. Borrás, A. R. González-Elipe, C. López-Santos, *Appl. Mater. Today* **2020**, *21*, 100815.
[40] L. Li, B. Li, J. Dong, J. Zhang, *J. Mater. Chem. A* **2016**, *4*, 13677.
[41] X. L. Gao, L. X. Sun, H. Y. Wu, Z. Y. Zhu, N. Xiao, J. H. Chen, Q. Yang, Q. G. Zhang, A. M. Zhu, Q. L. Liu, *J. Mater. Chem. A* **2020**, *8*, 13065.
[42] R. Sandström, A. Annamalai, N. Boulanger, J. Ekspong, A. Talyzin, I. Mühlbacher, T. Wågberg, *Sustainable Energy Fuels* **2019**, *3*, 1790.
[43] W. Wang, X. Du, H. Vahabi, S. Zhao, Y. Yin, A. K. K. T. Tong, *Nat. Commun.* **2019**, *10*, 3220.
[44] P. Zhu, T. Kong, X. Tang, L. Wang, *Nat. Commun.* **2017**, *8*, 15823.
[45] C. Li, X. Li, X. Du, T. Tong, T. Y. Cath, J. Lee, *ACS Appl. Mater. Interfaces* **2019**, *11*, 18456.
[46] R. Zheng, Y. Chen, J. Wang, J. Song, X.-M. Li, T. He, *J. Membr. Sci.* **2018**, *555*, 197.
[47] Z. Zuo, R. Liao, X. Song, X. Zhao, Y. Yuan, *RSC Adv.* **2018**, *8*, 19906.
[48] Y. Wang, L. Zhu, C. Du, *Adv. Mater. Interfaces* **2020**, *7*, 1901932.
[49] S. A. Chowdhury, M. C. Saha, S. Patterson, T. Robison, Y. Liu, *Adv. Mater. Technol.* **2019**, *4*, 1800398.
[50] Z. Guo, C. Sun, J. Zhao, Z. Cai, F. Ge, *Adv. Mater. Interfaces* **2021**, *8*, 2001695.
[51] F.-C. Liang, Y.-W. Chang, C.-C. Kuo, C.-J. Cho, D.-H. Jiang, F.-C. Jhuang, S.-P. Rwei, R. Borsali, *Nanoscale* **2019**, *11*, 1520.
[52] H. Zhang, A. U. Mane, X. Yang, Z. Xia, E. F. Barry, J. Luo, Y. Wan, J. W. Elam, S. B. Darling, *Adv. Funct. Mater.* **2020**, *30*, 2002847.
[53] M. Sun, I. Zucker, D. M. Davenport, X. Zhou, J. Qu, M. Elimelech, *Environ. Sci. Technol.* **2018**, *52*, 8674.
[54] A. Li, G. Wang, Y. Ma, C. Zhao, F. Zhang, Q. He, F. Zhang, *J. Mater. Res. Technol.* **2021**, *11*, 135.
[55] A. Jishnu, J. S. Jayan, A. Saritha, A. S. Sethulekshmi, G. Venu, *Colloids Surf., A* **2020**, *606*, 125395.
[56] A. Baidya, S. K. Das, R. H. A. Ras, T. Pradeep, *Adv. Mater. Interfaces* **2018**, *5*, 1701523.
[57] W. S. Y. Wong, T. P. Corrales, A. Naga, P. Baumli, A. Kaltbeitzel, M. Kappl, P. Papadopoulos, D. Vollmer, H. J. Butt, *ACS Nano* **2020**, *14*, 3836.
[58] A. Borrás, J. Cotrino, A. R. González-Elipe, *J. Electrochem. Soc.* **2007**, *154*, P152.
[59] A. N. Filippin, M. Macias-Montero, Z. Saghi, J. Idígoras, P. Burdet, J. R. Sanchez-Valencia, A. Barranco, P. A. Migdley, J. A. Anta, A. Borras, *Sci. Rep.* **2017**, *7*, 9621.
[60] A. N. Filippin, M. Macias-Montero, Z. Saghi, J. Idígoras, P. Burdet, A. Barranco, P. Midgley, J. A. Anta, A. Borras, *Sci. Rep.* **2016**, *6*, 20637.
[61] M. Alcaire, A. N. Filippin, M. Macias-Montero, J. R. Sanchez-Valencia, T. C. Rojas, A. Mora-Boza, C. Lopez-Santos, J. P. Espinos, A. Barranco, A. Borras, *Plasma Processes Polym.* **2016**, *13*, 287.